energies

MDPI

Article

Molecular Dynamics Simulation of CO_2 Diffusion in a Carbonated Water–Decane System

Lei Yuan, Changzhong Zhao, Yongsheng Xu and Yi Zhang *

Key Laboratory of Ocean Energy Utilization and Energy Conservation of Ministry of Education, School of Energy and Power Engineering, Dalian University of Technology, Dalian 116024, China; yuanlei@mail.dlut.edu.cn (L.Y.); stickzhong@mail.dlut.edu.cn (C.Z.); yongsheng@mail.dlut.edu.cn (Y.X.)
* Correspondence: zhangyi80@dlut.edu.cn

Received: 19 October 2020; Accepted: 16 November 2020; Published: 18 November 2020



Abstract: Carbonated water injection (CWI) is a technology with significant sweep efficiency advantages in enhanced oil recovery (EOR), but the mechanism of the microscopic diffusion of CO_2 is still unclear. In this study, the diffusion mechanism of CO_2 from the aqueous phase to the oleic phase in a carbonated water (CW)–decane system was investigated by the molecular dynamics simulation method. This investigation also explored the diffusion capacity and interface properties of the CW–decane system. We found that the movement of CO_2 from the aqueous phase to the oleic phase can be divided into two processes: the accumulation behavior of CO_2 moving from the aqueous phase to the interface, and the dissolution behavior of CO_2 moving from the interface to the decane phase. The increase in the temperature and CO_2 concentration in carbonated water can improve the decane phase's diffusion ability and reduce the water–decane interfacial tension. The difference in the interactions between water–CO_2 and decane–CO_2 provides a driving force for the diffusion of CO_2 between aqueous and oleic phase. The temperature increase intensifies the degree of diffusion and improves the diffusion rate of CO_2 from the aqueous phase to the oleic phase. The diffusion coefficient results show that CO_2 significantly enhances the oleic phase's diffusion properties. In addition, the affinity of water for CO_2 is increased by the hydrogen bond, and it provides a mechanism for the accumulation behavior of CO_2. Further, the temperature significantly improves the CO_2 diffusion ability at the interface, which promotes CO_2 leaving the interface and weakens the accumulation behavior. This work provides useful information for guiding carbonated water injection to improve the recovery mechanism of enhanced oil.

Keywords: carbonated water; CO_2 diffusion; interface; molecular dynamics simulation

1. Introduction

Injecting CO_2 into depleted oil and gas reservoirs is a common method to enhance crude oil recovery [1]. However, CO_2 has unfavorable properties, such as a higher mobility than crude oil, a density difference from crude oil, and gravity separation, which causes a higher residual oil saturation and lower sweep efficiency [2–7]. To overcome the above deficiencies in the process of pure CO_2 injection, methods such as water alternating gas, CO_2 foam flooding, simultaneous water alternating gas, and carbonated water injection (CWI) have been proposed [3,8,9].

Unlike other methods, CWI technology uses saturated CO_2 water to displace formed crude oil, which has the advantages of gas injection and water injection (WI). CWI is less affected by reservoir heterogeneity, which leads to a higher sweep efficiency [10,11], and it significantly reduces the residual oil saturation and improves the oil recovery [12]. In addition, the traditional CO_2 injection and WAG require continuous injection for a large amount of CO_2, which leads to the economic decline of many

reservoir projects. In contrast, the amount of CO_2 required by CWI is relatively small, which provides a feasible strategy for many reservoirs [13].

The first CWI commercial application was the K&S project in Oklahoma in the 1960s [14]. However, due to the economic reduction of the CO_2 acquisition's costs, it was eventually terminated. Recently, CWI has received attention because it provides additional oil recovery and CO_2 utilization. The feasibility of CWI technology has been verified in theory and through pilot tests. By studying sand-packs and core samples, the final recovery of crude oil was determined to be higher than water injection (WI) when CWI is used in secondary or tertiary injections [15,16]. Moreover, CO_2 is gradually dissolved in crude oil during the displacement process, which is conducive to the storage of CO_2 [16]. However, the unclear mechanism of enhanced oil recovery (EOR) and the potential of increasing production have restricted the popularization and application of this technology. Thus, the key scientific issues, which include the change in the basic physical properties and the diffusion process of CO_2 between phases, should be addressed urgently. These problems largely determine the effect on the EOR and CO_2 storage. Presently, it is generally believed that the main mechanism by which CWI improves the recovery is that which involves CO_2 diffusion causing the crude oil to become more mobilized. The flow of the reservoir fluid is strongly affected by the CO_2 diffusion, resulting in changes in the fluid properties, especially mobility, density, and interfacial tension (IFT), which reduces the residual oil saturation. Mostafa et al. [5] measured the interfacial tension between the different types of crude oil and CW, and they determined that the CO_2 reduces the pH of the system, which enhances the ionization of the alkaline surfactants in crude oil. Seyyedi et al. [17,18] conducted a series of experiments at high temperatures and high pressures, and found that, during the contact of CW with live oil, the transfer of CO_2 leads to the formation of a new phase. These new phases reconnect the captured oil, thereby increasing the recovery factor.

However, the current observation methods are not very clear in terms of the microscopic mechanism of CO_2 migration, changes of the oleic phase properties, and factors that affect the water–oil interface. Comprehensive descriptions of the microscopic mechanism after the CW contacts the oleic phase are scarce. In addition, the current mathematical model cannot accurately describe the CWI process [13,19].

As a fast-developing emerging technique, molecular dynamics simulation (MD) is used increasingly in the study of CO_2 geological storage and EOR [20–23]. It can help us better understand the interaction between the substances at the micro level. Zhang et al. [24] found that the swelling coefficient for CO_2-saturated octane is linearly related to the solubility of CO_2. Zhang et al. identified this by studying the solubility of CO_2 in the CO_2–octane system and the swelling of octane. Yang et al. [25] used direct interface simulation technology to analyze the interfacial tension of the NaCl–CO_2–water system and explored the variation of the interfacial tension in regard to temperature, pressure, and salinity. Dai et al. [26] studied the CO_2–water–butane system with MD to predict the phase equilibrium, and the calculated results agreed well with the experimental results. Liu et al. [27] studied the distribution of supercritical CO_2 in the water–oil system and determined that CO_2 was enriched at the interface. Although MD techniques have been used to detect the microscopic behavior of CO_2–water–oil systems under reservoir conditions, research on the phase behavior and interface characteristics of CW and oil systems is very limited. In addition, the microscopic process of CW contacting oil and the diffusion process of CO_2 from the aqueous phase to the oleic phase have not been reported on.

Therefore, this study uses MD to investigate the microscopic behavior of CW when it is in contact with oil. This study aims to further understand the transport mechanism of CO_2 during the CWI process, the effect of CO_2 on the CW–oil interface's characteristics, and the effect of CW–oil contact on the mobility of the oleic phase. The rest of this paper is structured as follows: Section 2 describes the details of MD and the calculation method. Then, Section 3 discusses the diffusion and distribution of CO_2 in the system after the CW–oil contact, and explains the microscopic mechanism through the diffusion properties, interface characteristics, and molecular interactions of the system. Section 4 presents the conclusion of this study. This work is helpful in better understanding the

mechanism of CWI in the reservoir that enhances the recovery and provides a basis for scientific and industrial research.

2. Simulation Method

2.1. Simulation Details

The open source package "LAMMPS" [28] was used to perform parallel computing. The simulation system contains three substances: water, CO_2 and decane (an alkane widely used to simulate the oleic phase). The water, CO_2, and decane were modeled using SPC/E [29], EPM2 [30], and OPLS-AA force field [31]. SPC/E is a widely recognized model for water molecules, and it has excellent predictive capabilities for the thermodynamic properties, time-varying properties, and phase equilibrium. The EPM2 model describes the thermodynamic properties of CO_2, especially in the near-critical region. OPLS-AA force field is suitable for the condensed nature of organic solvents. Additional model parameters are described in detail in Table S1 (in the supplementary material). The energy form of the system is described as follows:

$$E = E_{bond} + E_{angle} + E_{dihedral} + E_{vdW} + E_{ele} \quad (1)$$

where E is the total energy, E_{bond} is the bond stretching interaction, E_{angle} is the angle bending interaction, $E_{dihedral}$ is the dihedral torsioning interaction, E_{vdW} is the van der Waals (vdW) interaction, and E_{ele} is the coulomb interaction. Water molecules and CO_2 molecules are treated as rigid bodies by the SHAKE algorithm [32]. The non-bonding vdW interaction when using the Lennard-Jones 12-6 function and the coulomb interaction are described as follows:

$$E_{ij} = 4\varepsilon_{ij}\left[\left(\frac{\sigma_{ij}}{r_{ij}}\right)^{12} - \left(\frac{\sigma_{ij}}{r_{ij}}\right)^{6}\right] + \frac{q_i q_j}{r_{ij}} \quad (2)$$

where r_{ij} is the distance between atom i and atom j, ε and σ represent the vdW interaction parameter, and q is the atomic charge. The particle-particle particle-mesh (PPPM) algorithm [33] was used for the long-range Coulombic interaction, while the cutoff for the short-range interaction was set to 14 Å. The parameters between dissimilar molecules were mixed with geometric rules, as follows:

$$\varepsilon_{ij} = \sqrt{\varepsilon_i \varepsilon_j} \quad (3)$$

$$\sigma_{ij} = \sqrt{\sigma_i \sigma_j} \quad (4)$$

The initial configuration of the simulation box consists of three parts, including two CW regions and one oil region, as shown in Figure 1. Each CW region includes 4000 water molecules and 0, 34, and 68 CO_2 molecules, which corresponds to a CW flow with a CO_2 mass fraction (ωCO_2) of 0.0%, 2.0%, and 4.0%, respectively. The oleic phase includes 400 decane molecules. Each region is set as an orthogonal box in which the dimensions are $L_x \times L_y \times L_z$, where $L_x = L_y = 4$ nm, and L_z is determined by the density of the solution, which is about 8 nm. Periodic boundaries were used in all of the dimensions. The box is large enough to completely observe the CO_2 diffusion between the phases.

At the initial configuration of the system, each region was separately relaxed by 2 ns to reach the set temperature and pressure to ensure a uniform distribution of the system, then the three regions were spliced according to the interface (a more detailed relaxation process is described in the supplementary material). According to the Gaussian distribution, the initial atomic velocity of the spliced system was reset to the desired temperature. By modifying the random number of the atomic velocity, three repeated experiments were carried out in each condition. Thereafter, the CW–decane system was simulated for 30 ns under the isothermal–isobaric ensemble (NPT), with the Nose–Hoover method [34]. The simulation runs with a time step of 1 fs, and atom trajectories were dumped once per 1000 fs for the required statistical results.

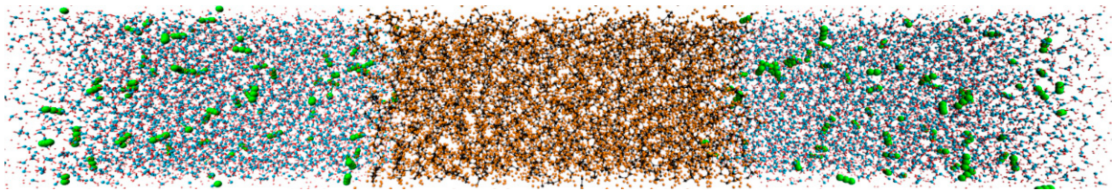


Figure 1. Perspective drawing of the CW–decane system at 353 K and 20 MPa. C (decane), H (decane), O (water), and H (water) are represented by black, orange, blue, and red spheres, respectively. C and O in CO_2 are represented by green spheres.

2.2. Calculation Methods

The density profile was calculated by dividing the simulation box into slices with a thickness of 1Å along the *z*-axis, as shown in Figure 2a. We determined the interface of the CW–decane according to the Gibbs dividing surface (GDS) [35], where the atom number of excess decane in the aqueous phase was almost the same as the atom number of excess water in the oleic phase. Owing to the discontinuity at the CW–decane interface, the density profile at the interface could be fitted as an empirical hyperbolic tangent function (tanh) [36] as follows:

$$\rho(z) = \frac{1}{2}(\rho_W + \rho_O) - \frac{1}{2}(\rho_W + \rho_O)\tanh[(z - z_0)/d] \tag{5}$$

where ρ_W and ρ_O represent the density of the water and oleic phase away from the interface, z_0 represents the position of the water–decane interface, and d is a fitting parameter related to the interface width. The "10–90" rule [37] was used to determine the interface width Δz, i.e., $\Delta z = 2.1972d$.

The interfacial tension (IFT), which is an important property of the phase interface, can be calculated by the diagonal element of the pressure tensor P_{xx}, P_{yy}, and P_{zz} as follows:

$$\gamma = \frac{L_z}{2}[\langle P_{zz}\rangle - \frac{1}{2}\left(\langle P_{xx}\rangle + \left\langle P_{yy}\right\rangle\right)] \tag{6}$$

where L_z is the size of the box in the *z*-axis direction, $\langle\ \rangle$ represents an ensemble average. The time period after system equilibrium is divided into several blocks to estimate the uncertainty of the results.

The diffusion coefficient (D) can be obtained by calculating the mean square displacement as follows:

$$D = \frac{1}{6}\lim_{t\to\infty}\frac{d}{dt}\sum_{i}^{n}\left\langle\left|R_i(t) - R_i(0)\right|^2\right\rangle \tag{7}$$

where $R_i(t)$ is the coordinate of the atom i at time t, and $R_i(0)$ is the coordinate of the i atom at time 0.

The interaction energies between two components can be calculated by Equation (8):

$$E_{\mathrm{A-B}} = E_{\mathrm{AB}} - E_{\mathrm{A}} - E_{\mathrm{B}} \tag{8}$$

where E_{AB} is the total energy of the whole system containing components A and B, and $E_A$and E_B are the energy of components A and B, respectively.

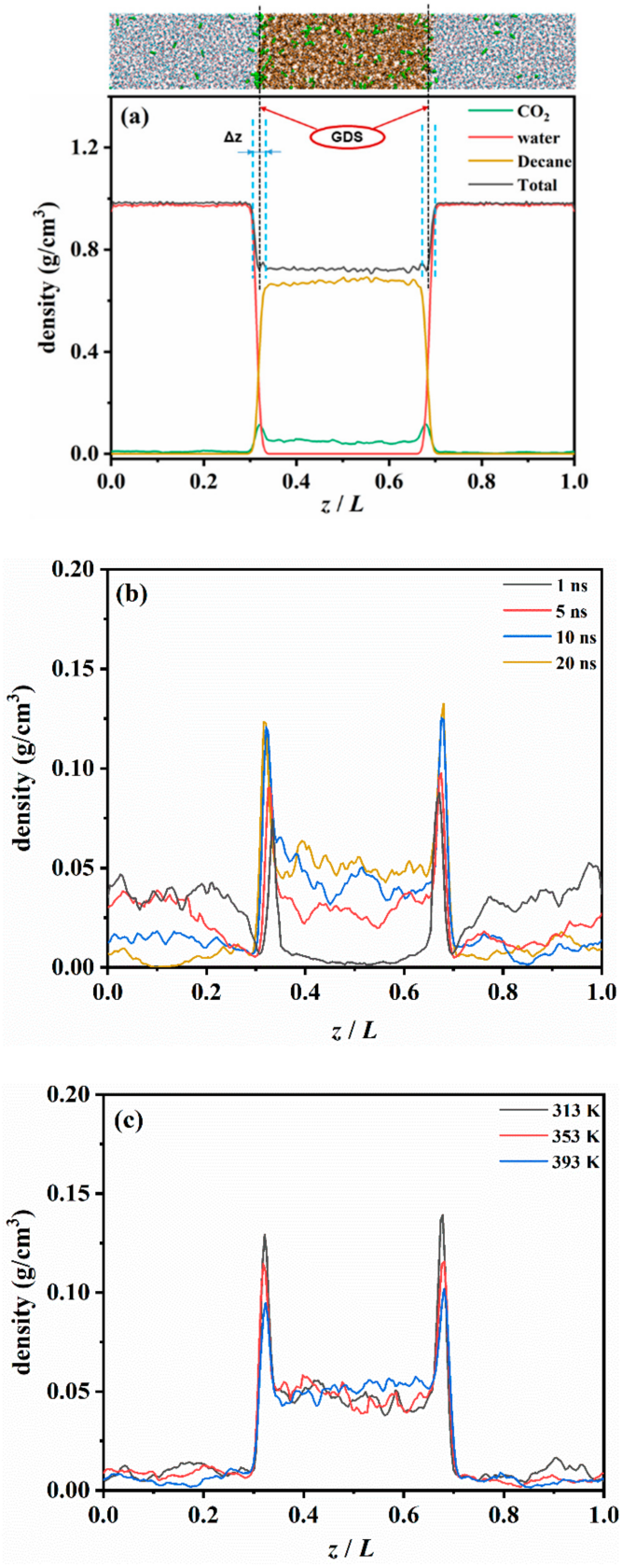


Figure 2. Density profile along the interface direction (z axis) of the CW-decane system with 4% ωCO_2. (**a**) Equilibrium distribution of each component at 353 K and 20 MPa. (**b**) Time-varying distribution of CO_2 at 353K and 20 MPa. (**c**) The effect of temperature on the CO_2 distribution after the CW–decane system reaches equilibrium at 20 MPa.

3. Results and Discussion

3.1. CO_2 Diffusion Behavior after Phases Contact

3.1.1. Diffusion Process and Distribution of CO_2

To quantitatively describe the distribution of CO_2 in the diffusion process, the density profiles of each component along the vertical interface direction (z axis) were calculated. The results of the water–decane binary system were compared with the National institute of standards and technology (NIST) database to prove the reliability of the calculation results (see Table S1 in the Supplementary Materials for more details).

Figure 2b shows the diffusion of CO_2 from the aqueous phase to the oleic phase after the phases contact each other. The figure illustrates that, at 1 ns, basically no CO_2 exists in the oleic phase. However, the density curve has a noticeable peak at the interface, which implies that a large amount of CO_2 is accumulated at the water–oil interface. As the contact time progressed, the amount of CO_2 in the oleic phase continued to increase, and the peak value at the interface also increased. In addition, the peak growth rate was rapid at the beginning and then gradually slowed down. This implies that the CO_2 at the interface gradually reached saturation. Finally, the peak value fluctuated slightly within a certain range before the system reached equilibrium. The above phenomenon shows that the diffusion of CO_2 from the aqueous phase to the oleic phase can be divided into two processes. The first process is the accumulation behavior of the CO_2 in the CW's move towards the interface. The second one is the dissolution behavior of the CO_2 at the interface moving towards the oleic phase. This can be observed from the accumulation rate of CO_2 at the interface. During the initial stage of diffusion, the diffusion of CO_2 was mainly based on the accumulation behavior. The increase in the concentration of CO_2 at the interface also enhanced the dissolution of CO_2 into the oil, and the two processes were mostly synchronized in time thereafter.

Figure 2a shows the density profile of the CW–decane system after equilibrium. The density profile results show that the peak of the CO_2 curve at the water–oil interface was about 0.114g/cm^3, while in the aqueous and decane phases, it was 0.008 and 0.047 g/cm^3, respectively. When the system is in equilibrium, the distribution of CO_2 in the CW–decane system has the order of interface > oleic phase > aqueous phase. A large number of CO_2 molecules tend to accumulate at the CW–decane interface, which will have a significant effect on the interface properties. In addition, the distribution of CO_2 in the CW–decane system also demonstrates that the solubility of CO_2 in the oleic phase is stronger than in the aqueous phase. When the system reaches equilibrium, even if the solubility of CO_2 in the oleic phase is not saturated (CO_2 concentration is far from saturated solubility), the CO_2 in the aqueous phase will not continue to move to the oleic phase. The CO_2 distribution between the aqueous and oleic phases according to a certain partition coefficient (k_{pc}) [11], which reflects the diffusion degree of CO_2 to the oleic phase, is presented in Table 1. The calculation results are in good agreement with the previous experiments [11,38,39]. When the temperature rose from 313 K to 393 K, k_{pc} increased from 4.22 to 7.25. This implies that the increase in temperature enhanced the diffusion degree of CO_2 from the aqueous phase to the oleic phase, which is beneficial to transferring CO_2 to the oleic phase.

Table 1. Partition coefficients of CO_2 in the CW–decane system with 4% ωCO_2 at 20 MPa.

T (K)	k_{pc}
313	4.22
353	5.98
393	7.25

3.1.2. Mechanism of CO_2 Diffusion Process

The diffusion of CO_2 in the CW–decane system could be described by the changing intermolecular interaction; thus, the interaction energy of water–CO_2 ($E_{water\text{-}CO_2}$) and decane–CO_2 ($E_{decane\text{-}CO_2}$) was calculated. Figure 3 shows how the $E_{water\text{-}CO_2}$ and $E_{decane\text{-}CO_2}$ change with time at different temperatures. At 1 ns, the $E_{water\text{-}CO_2}$ at 313 K was −713 kcal/mol, which is much greater than the –121.825 kcal/mol for $E_{decane\text{-}CO_2}$. The results show that, in the initial stage, the interaction between decane and CO_2 was very weak. At this stage, CO_2 mainly depends on its self-diffusion ability to move in the aqueous phase. When CO_2 moves to the near-interface area, it will accumulate at the interface due to the combined action of water and decane. In the next 2–20 ns, the $E_{water\text{-}CO_2}$ decreased rapidly, while $E_{decane\text{-}CO_2}$ increased significantly. This was the main period for the diffusion of CO_2 from CW to decane. The concentration of CO_2 on the front edge of the aqueous phase decreased, which caused the CO_2 in the aqueous phase to move continuously to the region near the interface. Finally, the $E_{water\text{-}CO_2}$ and $E_{decane\text{-}CO_2}$ no longer changed, but a small fluctuation existed, which showed that the CO_2 was in equilibrium in the system. After equilibrium, the $E_{decane\text{-}CO_2}$ was larger than the $E_{water\text{-}CO_2}$, which shows that the water and decane remained attractive to CO_2, which caused the CO_2 to be distributed into two phases. However, the interaction between CO_2 and decane was stronger; thus, the CO_2 preferred to dissolve in the oleic phase. In addition, the temperature rise reduced the $E_{water\text{-}CO_2}$ after the system reached equilibrium, and this increased the $E_{decane\text{-}CO_2}$. This implies that the temperature promoted the diffusion of CO_2 from the aqueous phase to the oleic phase. This clarifies the reason why the partition coefficient k_{pc} increased with temperature from the micro level.

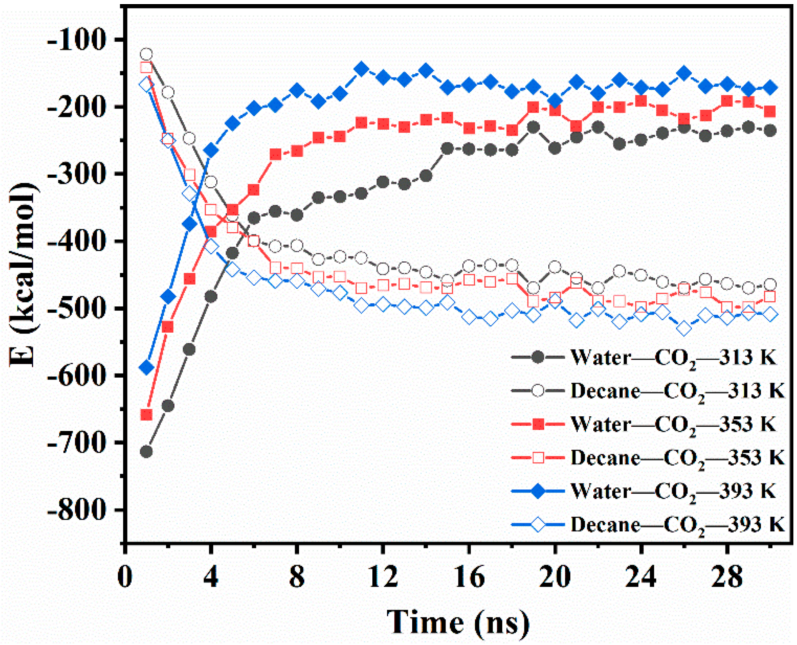


Figure 3. Intermolecular energetic interactions for the CW–decane system with 4% ωCO_2 at 20 MPa as a function of time.

From the microscopic contact process of the CW–decane system, it can be observed that after contact, the CO_2 in the aqueous phase tended to diffuse into the oleic phase, and a large amount of CO_2 accumulated at the water–oil interface during the diffusion process. This has an important effect on the properties of the oleic phase and the CW–decane interface. In addition, this further affects the oil recovery in the process of CO_2–EOR.

3.2. CO_2 Diffusion Coefficient and Its Effect on Phase Diffusivity

Determining the diffusion coefficient (D) for each component in a multi-component system is a challenge. However, by using MD techniques, we can directly determine the transport properties of each component under a variety of thermodynamic conditions in a complex system. To further study the diffusion ability of CO_2 after phase contact, D_{CO_2} under different temperature conditions was explored.

3.2.1. The D_{CO_2} along the Vertical Interface Direction

While considering the anisotropy of CO_2 diffusion in the system, the one-dimensional diffusion of CO_2 in the direction vertical to the interface (z axis) was studied. As shown in Figure 4, D_{CO_2} had an increasing trend at the beginning. This implies that the accumulation behavior of the initial stage promotes the diffusion of CO_2. With the continuous transfer of CO_2 in the medium-term of diffusion, D_{CO_2} shows a downward trend. During this period, a large amount of CO_2 dissolves into decane, and the deepening of the diffusion gradually weakens the driving force. Finally, the CO_2 reaches a dynamic equilibrium in the system and D_{CO_2} is unchanged. The temperature increase causes an evident rise in the initial diffusivity of CO_2 between the two phases. In addition, the higher the temperature, the earlier the curve falls, and the system reaches equilibrium sooner. At a temperature of 393 K, the diffusion curve drops rapidly, and the system reaches equilibrium at 16 ns. At 353 K, equilibrium is reached at 25 ns. At a temperature of 313 K, the D_{CO_2} decreased slowly with time. Compared to 353 K, the equilibrium time at 393 K was reduced by 36%. In summary, we believe that CO_2 is affected by the difference in the interaction between water–CO_2 and decane–CO_2, and causes CO_2 to continue diffusing into the oleic phase. Because the movement of CO_2 during the initial stage of diffusion enhances the interaction between CO_2 and decane, the initial diffusion rate increases. Then, with the continuous diffusion of CO_2, the driving force caused by the interaction difference is weakened, and the diffusivity gradually decreases until the system reaches equilibrium.

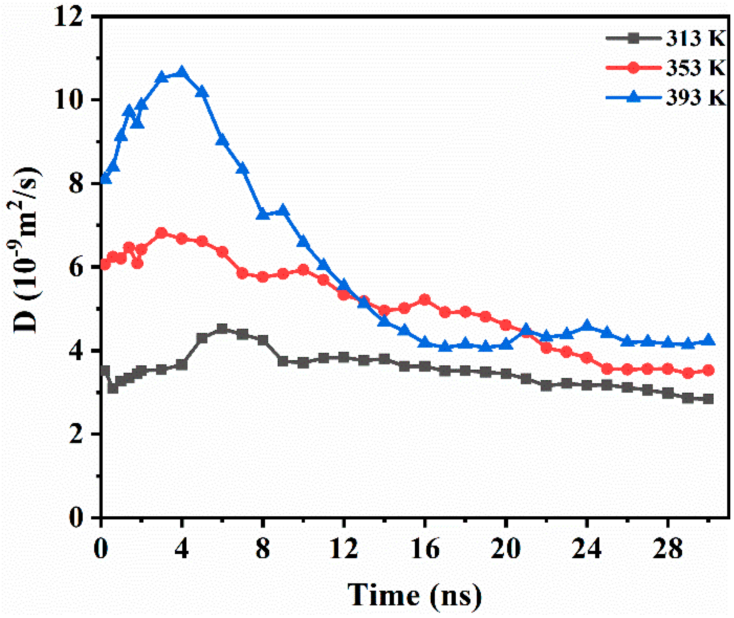


Figure 4. D_{CO_2} along the interface direction (z axis) while varying with time for the CW–decane system with 4% ωCO_2 at 20 MPa.

3.2.2. The D_{CO_2} in Different Regions of the CW–Decane System

It is worth noting that the concentration of CO_2 starts to decrease from the front edge of the aqueous phase during diffusion (Figure 2b); however, the CO_2 at this position is not completely exhausted.

This indicates that CO_2 has a good transport capacity in the aqueous phase during diffusion [40]. This allows CO_2 in the aqueous phase to diffuse to the interface continuously. We determined that, when the CO_2 leaves the interface under the attraction of decane, it diffuses rapidly in the oleic phase. This makes the distribution of CO_2 in the oleic phase more uniform than in the aqueous phase, indicating that the diffusion capacity of CO_2 in oil may be stronger in the aqueous phase. Therefore, the diffusion capacity of the different locations in the system was evaluated.

The D_{CO_2} in the aqueous phase, the interface, and the oleic phase was calculated by selecting different regions in the system. The thickness of each calculation region in the aqueous and oleic phases was 3 nm, and that of the calculation area at the interface was Δz, which is provided in Table 2. The results are presented in Figure 5. It can be observed that the D_{CO_2} in the oleic phase was significantly higher than that in the aqueous phase. Fang [41] indicated that there are voids in the oleic phase that are not occupied by decane molecules due to the entanglement of the alkane chains, which is defined as a free volume. CO_2 can rapidly penetrate into the free volumes, which are larger than the molecular volume of CO_2. Adjacent free volume connections can form tiny channels in the oleic phase, which helps CO_2 move rapidly into the oleic phase [41]. In addition, there is an extra hydrogen bond (H-bond) interaction between water and CO_2, which will weaken the diffusion capacity of CO_2 in water [42]. Furthermore, the temperature effect on the D_{CO_2} at the interface was more noticeable. At 313 K, D_{CO_2} at the interface was similar to that in the oleic phase, and when the temperature rose to 393 K, the D_{CO_2} at the interface was greater than that in the oleic phase. This implies that, at high temperatures, the activity of CO_2 at the interface is stronger, which will promote CO_2 to leave the interface and transfer to the oleic phase.

Table 2. Calculated results of the diffusion coefficient and the interfacial properties after the CW–oil system equilibrium at 20 MPa.

T	ωCO_2 (%)	D_{water} (10^{-9} m^2/s)	D_{decane} (10^{-9} m^2/s)	γ (mN/m)	Δz (Å)
313	4	3.367 ± 0.019	0.954 ± 0.018	53.83 ± 1.68	5.72 ± 0.10
353	0	5.314 ± 0.026	1.329 ± 0.027	52.51 ± 1.53	4.85 ± 0.07
-	2	5.372 ± 0.016	1.386 ± 0.030	50.29 ± 1.61	5.42 ± 0.05
-	4	5.384 ± 0.027	1.497 ± 0.035	49.16 ± 1.91	6.00 ± 0.14
393	4	7.970 ± 0.051	2.142 ± 0.046	45.62 ± 2.11	6.41 ± 0.13

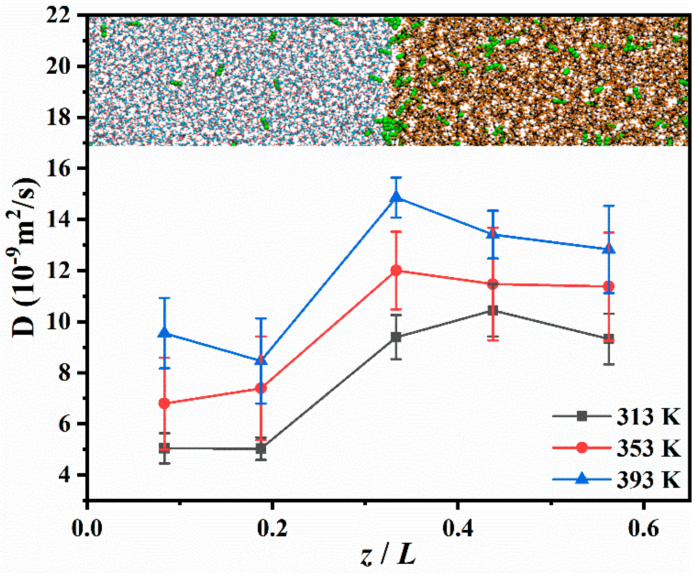


Figure 5. D_{CO_2} at different locations in the CW–decane system with 4% ωCO_2 at 20 MPa.

3.2.3. Effect of CO_2 on Diffusivity of Oleic Phase

The self-diffusion coefficients of the aqueous phase and the oleic phase were calculated and the effect of temperature and CO_2 concentration were explored on the diffusion capacity of the CW–decane system. The results are displayed in Table 2. The results of the comparison with others' experiments are shown in Figures S1 and S2 [43–45].

The increase in temperature renders the thermal motion of the molecules more intense and enhances the diffusion ability of the molecules. The temperature has a significant effect on the diffusivity of the water phase and the oleic phase. When the temperature increased from 313 K to 393 K, the diffusion coefficient of the water phase increased from 3.367×10^{-9} m^2/s to 7.970×10^{-9} m^2/s, while the oleic phase increased from 0.954×10^{-9} m^2/s to 2.142×10^{-9} m^2/s. Meanwhile, as the concentration of CO_2 in carbonated water increased, the diffusivity of the oleic phase also increased. The CW of 4% ωCO_2 increased the oleic phase's diffusion coefficient from 1.329×10^{-9} m^2/s to 1.497×10^{-9} m^2/s, an increase of approximately 12%. However, the change in the diffusion capacity of the aqueous phase was very small. From this, it is seen that increasing the CO_2 concentration in CW will not have a significant impact on the mobility of CW; however, diffusing CO_2 into the oleic phase can reduce the viscosity of the oleic phase and improve the mobility of the oleic phase.

3.3. CO_2 Accumulation and Its Effect on the CW–Decane Interface

During the diffusion of CO_2 from the aqueous phase to the oleic phase, it will not be precipitated as free gas, and the phenomenon of accumulation at the interface will be observed. This will change the nature of the water–oil interface and affect the efficiency of CWI. Sohaib [46] demonstrated that the difference in the IFT between water–CO_2 and water–decane results in the accumulation of CO_2. However, its microscopic mechanism has not yet been elucidated. Therefore, the mechanism of CO_2 accumulation behavior and its impact on the interface properties was studied in this work.

3.3.1. Interfacial Tension of the CW–Decane Interface

The IFT of the CW–decane interface was analyzed to express the effect of the CO_2 concentration and temperature on the IFT through five sets of experiments. As indicated in Table 2, the IFTs agree well with the previous studies [47,48].

Compared with pure water, the CW with 2% ωCO_2 reduced the IFT from 52.51 mN/m to 50.29 mN/m at 353 K. With a higher CO_2 concentration, there was a more noticeable decrease in the IFT. When the CW was 4% ωCO_2, it dropped to 49.16 mN/m. This shows that CWI has less IFT after contact with oil than WI, which provides a higher recovery potential. The increase in temperature will also reduce the IFT of CW–oil, and similar conclusions have been reported [49]. We determined that as the temperature increases, the peak CO_2 at the interface decreases, as shown in Figure 2c. The increase in temperature weakens the CO_2 accumulation behavior. This is because the increase in temperature significantly increases the diffusion capacity of CO_2 in the interfacial region. This also enhances the CO_2 leaving the interface as it diffuses into the oleic phase, thus reducing the peak CO_2. The reduction in CO_2 concentration at the interface weakens the effect of CW to reduce the interfacial tension. However, the CO_2 accumulation behavior at the CW–decane interface is similar to that of aromatic hydrocarbons [50], which act as a surfactant. The increase in temperature increases the activity of CO_2, which promotes the reduction of IFT.

Due to the strong hydrophobicity of alkanes, there is a clear interface between the aqueous and oleic phases. Therefore, the variation for the CW–decane interface width, Δz, was explored, as shown in Table 2. The calculation results show that when CO_2 accumulates at the water–oil interface, the interface becomes wider under the influence of CO_2. In addition, the increase in the CO_2 concentration and temperature makes the Δz increase more noticeable. The increase in Δz implies that the two-phase molecules penetrate each other, which is beneficial for reducing IFT.

3.3.2. Structural Properties of CW–Decane Interface

The change in the IFT is a result of the change in the interface structural properties; thus, we explore the structural properties in the interface region to explain the IFT change.

Figure 6 describes the radial distribution function (RDF) of the water–decane molecules at the interface at 353 K and 20 MPa. It can be observed that the two curves have only one peak, and no second peak appears. This implies that, at the interface, the water–decane molecules showed a loose and disordered structure. When the CO_2 concentration was 0%, the first peak of the RDF was located at 4.35 Å with an amplitude of 21.5. When the CO_2 concentration was 4%, the first peak of the RDF was located at 4.75 Å with an amplitude of 19.4. The presence of CO_2 at the interface made the amplitude lower and the position of the peak increased. The RDF describes the probability that a decane molecule is present at a distance r from a water molecule. The possibility decreases with an increasing CO_2 concentration. This shows that the accumulation behavior increases the average relative distance between the water and decane molecules. The solution structure at the interface was looser, which had an important effect on the reduction of the interfacial tension.

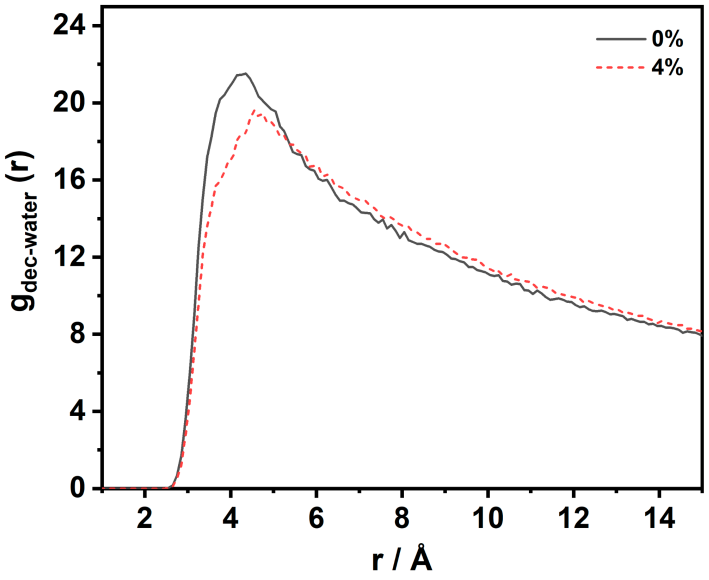


Figure 6. RDF of C (decane)–O (water) at the interfacial in the CW–decane system with a different CO_2 concentration at 353 K and 20 MPa.

The hydrogen bonds (H–bond) between the water molecules have an important influence on the structural strength of the solution. In liquid water, a dynamic H bond network can be formed, which also forms clusters of water molecules. This makes the connection between the water molecules closer, which affects the interfacial tension. Therefore, we explored the H bond number at the CW–decane interface. Given that the lifetime of H bonds is generally between 1–20 ps, 200 configurations were counted after system equilibrium and the time interval between each configuration was 10 ps. As shown in Figure 7, more H bonds were generated between water and CO_2 as the CO_2 concentration in the CW increased. Meanwhile, the number of H bonds between water molecules gradually decreased since the H bonds reached saturation. When the H bonds between the oxygen molecules in CO_2 and the hydrogen in water form, due to the mutual repulsion between the negative ions, the oxygen atom is more difficult to access for other water molecules. The above shows that the network structure between the water molecules at the interface is weakened by the influence of the CO_2 molecules, which reduces the interaction between the water molecules and promotes the mutual penetration of molecules at the interface. H bonds enhance the interaction and make the structure between water and CO_2 more stable, which is conducive to the accumulation behavior of CO_2.

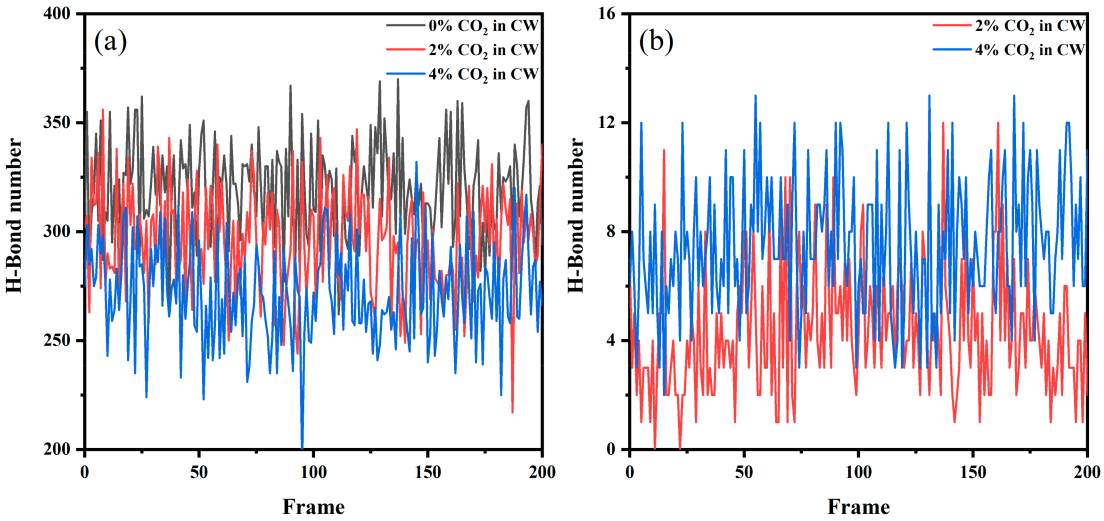


Figure 7. The number of H–bonds at the CW–decane interface at 353 K and 20 MPa: (**a**) between hydrogen (water) and oxygen (water) and (**b**) between hydrogen (water) and oxygen (CO_2).

3.3.3. Intermolecular Interactions

As shown in Table 3, we assessed the structural and energy change at the interface of the CW–decane system by determining the interaction between CO_2, water and decane with different CO_2 concentrations. When the CW was 0% ωCO_2, the $E_{water\text{-}water}$ was higher than the $E_{decane\text{-}decane}$; however, both were larger than the $E_{water–decane}$. This implies that the attraction of water and decane is weaker, which makes it difficult for water and decane to be miscible and form a stable interface. As the concentration of CO_2 increased, the $E_{water–decane}$ decreased, while the $E_{water\text{-}CO_2}$ and $E_{decane\text{-}CO_2}$ increased. This shows that the CO_2 at the interface does not play a role in enhancing the $E_{water–decane}$ to reduce the interfacial tension, but it acts as a bridge at the interface by enhancing the $E_{water\text{-}CO_2}$ and $E_{decane–CO_2}$. In addition, the $E_{water\text{-}CO_2}$ was slightly larger than the $E_{decane\text{-}CO_2}$. This is because the effect of the H bonds at the interface gives the water at the interface a stronger affinity for CO_2, which inhibits the movement of CO_2 to the oleic phase.

Table 3. Intermolecular energetic interactions (kcal/mol) in the interfacial region at 353 K and 20 MPa.

ωCO_2 (%)	Water–Water	Water–CO_2	Decane–Decane	Decane–CO_2	Water–Decane
0.0	−3349.2	0	−167.2	0	−67.1
2.0	−3257.4	−38.6	−177.0	−29.7	−58.1
4.0	−3266.9	−71.2	−176.1	−47.4	−50.61

In summary, the H bond effect makes the affinity of water for CO_2 stronger than for decane, which inhibits the diffusion of CO_2 to the oleic phase, causing an accumulation of CO_2 at the interface. Due to the saturation of the H bonds, the affinity of water for CO_2 is very limited. When the concentration of CO_2 at the interface gradually increases, CO_2 diffuses into the oleic phase. In addition, the formation of H bonds between CO_2 and water destroys the stable network structure of water. As such, decane can be further extended to the aqueous phase through CO_2 that is accumulated at the interface, which enhances the mutual permeability of water and decane, making the interface wider and reducing the IFT.

4. Conclusions

The molecular dynamics simulation method was used to study the CO_2 diffusion process in the CW–decane contact process. The effects of the CO_2 in the CW on the system's diffusion capacity and

the water–oil interfacial properties were also investigated. The results of the system density profile show that the diffusion of CO_2 from the aqueous phase to the oleic phase is mainly divided into two processes: the accumulation behavior of CO_2 moving from the aqueous phase to the interface, and the dissolution behavior of CO_2 moving from the interface to the oleic phase. The accumulation behavior was dominant at the start of the simulation. In most instances thereafter, the two behaviors were observed simultaneously. Once the system is in equilibrium, due to the fact that interaction of water with CO_2 is stronger than that of decane with CO_2, the partition coefficients of CO_2 in the oleic phase are higher than in the aqueous phase. Furthermore, the partition coefficients increase as the temperature rises.

By evaluating the diffusion properties of the system, the diffusion coefficients of the two phases were changed by CO_2. Compared with WI without CO_2, a CW with 4% ωCO_2 increased the diffusion capacity of the oleic phase by 12%; however, water phase enhancement was not evident. Specifically, the temperature has a significant effect on the CO_2 diffusion capacity of the system. The equilibrium time of the system at 353 K was 25 ns, whereas at 393 K, the equilibrium time was 16 ns, which is a reduction of nearly 36%. The diffusion coefficients of CO_2 in the oleic phase were stronger than those in the water phase. The reason is that the hydrogen bonds between CO_2 and water weaken the diffusion capacity of CO_2 in the aqueous phase, as well as the fact that the free volume in the oleic phase is beneficial for CO_2 diffusion.

Research on the properties of the CW–oil interface shows that the accumulation behavior of CO_2 during the diffusion process is caused by the hydrogen bonds between water and CO_2 enhancing water's affinity for CO_2. This inhibits the diffusion of CO_2 to the oleic phase, which causes CO_2 to accumulate at the interface. Due to the saturation of the hydrogen bonds, the attraction of the interface to CO_2 is limited. When the concentration of CO_2 at the interface increases, it continuously diffuses to the oleic phase. The formation of hydrogen bonds between water and CO_2 destroys the water network structure at the interface, and the decane molecules can further extend into the water phase through the CO_2 that is accumulated at the interface. This causes the structure within the interface to be looser and the mutual permeability of the two-phase molecules to be enhanced. As such, the interface width increases and the interface tension decreases. In addition, the temperature significantly improves the diffusion capacity of CO_2 in the interface region. It promotes the CO_2 moving from the interface into the oleic phases, and weakens the accumulation behavior of CO_2.

In summary, this study describes the dynamic process of CO_2 diffusion during CW–oil contact. This research describes important details about the transport properties and interface characteristics of the CWI process, which helps with the application of CWI to improve the recovery. However, in addition to aliphatic hydrocarbon chains, crude oil contains a large number of complex components such as aromatic hydrocarbons, resins, asphaltenes, and dissolved gases. Therefore, the effect of CW on multicomponent oil systems will be further considered in the future.

Supplementary Materials: The following are available online at http://www.mdpi.com/1996-1073/13/22/6031/s1, Figure S1: Water diffusion coefficient, Figure S2: Decane diffusion coefficient, Figure S3: Interface tension of water/decane, Table S1: Interatomic interaction parameters, Table S2: The density values of water phase and oil phase.

Author Contributions: Conceptualization, L.Y. and Y.Z.; methodology, L.Y.; software, L.Y.; validation, L.Y., C.Z. and Y.X.; formal analysis, Y.X.; investigation, L.Y.; resources, L.Y.; data curation, C.Z.; writing—original draft preparation, L.Y.; writing—review and editing, L.Y.; visualization, Y.X.; supervision, Y.Z.; project administration, Y.Z.; funding acquisition, Y.Z. All authors have read and agreed to the published version of the manuscript.

Funding: This research was funded by the National Natural Science Foundation of China (Grants 51976024), and the National Key R&D Program of China (Grants 2016YFB0600804).

Conflicts of Interest: The authors declare no conflict of interest.

References

1. Bui, M.; Adjiman, C.S.; Bardow, A.; Anthony, E.J.; Boston, A.; Brown, S.; Fennell, P.S.; Fuss, S.; Galindo, A.; Hackett, L.A.; et al. Carbon capture and storage (CCS): The way forward. *Energy Environ. Sci.* **2018**, *11*, 1062–1176. [CrossRef]
2. Riazi, M. Pore Scale Mechanisms of Carbonated Water Injection in Oil Reservoirs. Ph.D. Thesis, Heriot Watt University, Edinburgh, UK, 2011.
3. Nevers, N.H. Carbonated waterflooding: Is it a lab success and a field failure. *World Oil* **1966**, *163*, 93–96.
4. Seyyedi, M.; Mahzari, P.; Sohrabi, M. A comparative study of oil compositional variations during CO_2 and carbonated water injection scenarios for EOR. *J. Pet. Sci. Eng.* **2018**, *164*, 685–695. [CrossRef]
5. Lashkarbolooki, M.; Riazi, M.; Ayatollahi, S. Effect of CO_2 and natural surfactant of crude oil on the dynamic interfacial tensions during carbonated water flooding: Experimental and modeling investigation. *J. Pet. Sci. Eng.* **2017**, *159*, 58–67. [CrossRef]
6. Esene, C.; Rezaei, N.; Aborig, A.; Zendehboudi, S. Comprehensive review of carbonated water injection for enhanced oil recovery. *Fuel* **2019**, *237*, 1086–1107. [CrossRef]
7. Song, Y.; Zhao, C.; Chen, M.; Chi, Y.; Zhang, Y.; Zhao, J. Pore-scale visualization study on CO_2 displacement of brine in micromodels with circular and square cross sections. *Int. J. Greenh. Gas Control* **2020**, 95. [CrossRef]
8. Kulkarni, M.M.; Rao, D.N. Experimental investigation of miscible and immiscible Water-Alternating-Gas (WAG) process performance. *J. Pet. Sci. Eng.* **2005**, *48*, 1–20. [CrossRef]
9. Sohrabi, M.; Riazi, M.; Jamiolahmady, M.; Kechut, N.I.; Ireland, S.; Robertson, G. Carbonated Water Injection (CWI)—A productive way of using CO_2 for oil recovery and CO_2 storage. In *Proceedings of the 10th International Conference on Greenhouse Gas Control Technologies, Amsterdam, The Netherlands, 19–23 September 2010*; Gale, J., Hendriks, C., Turkenberg, W., Eds.; Elsevier: Amsterdam, The Netherlands, 2011; Volume 4, pp. 2192–2199.
10. Mosavat, N.; Torabi, F. Micro-optical analysis of carbonated water injection in irregular and heterogeneous pore geometry. *Fuel* **2016**, *175*, 191–201. [CrossRef]
11. Shu, G.; Dong, M.; Chen, S.; Hassanzadeh, H. Mass transfer of CO_2 in a carbonated water-oil system at high pressures. *Ind. Eng. Chem. Res.* **2017**, *56*, 404–416. [CrossRef]
12. Mosavat, N.; Torabi, F. Experimental evaluation of the performance of carbonated water injection (CWI) under various operating conditions in light oil systems. *Fuel* **2014**, *123*, 274–284. [CrossRef]
13. Kechut, N.I.; Jamiolahmady, M.; Sohrabi, M. Numerical simulation of experimental Carbonated Water Injection (CWI) for improved oil recovery and CO_2 storage. *J. Pet. Sci. Eng.* **2011**, *77*, 111–120. [CrossRef]
14. Hickok, C.W.; Ramsay, H.J., Jr. Case histories of carbonated waterfloods in Dewey-Bartlesville field. Case histories of carbonated waterfloods in Dewey–Bartlesville field. In Proceedings of the SPE Secondary Recovery Symposium, Wichita Falls, TX, USA, 7–8 May 1962.
15. Riazi, M.; Sohrabi, M.; Jamiolahmady, M.; Ireland, S.; Brown, C. Oil Recovery improvement using CO_2-enriched water injection. In Proceedings of the EUROPEC/EAGE Conference and Exhibition, Amsterdam, The Netherlands, 8–11 June 2009.
16. Mosavat, N.; Torabi, F. Application of CO_2-saturated water flooding as a prospective safe CO_2 storage strategy. In *Proceedings of the 12th International Conference on Greenhouse Gas Control Technologies, Ghgt-12, Austin, TX, USA, 5–9 October 2014*; Dixon, T., Herzog, H., Twinning, S., Eds.; Elsevier: Amsterdam, The Netherlands, 2014; Volume 63, pp. 5408–5419.
17. Seyyedi, M.; Mahzari, P.; Sohrabi, M. An integrated study of the dominant mechanism leading to improved oil recovery by carbonated water injection. *J. Ind. Eng. Chem.* **2017**, *45*, 22–32. [CrossRef]
18. Seyyedi, M.; Sohrabi, M. Pore-scale investigation of crude Oil/CO_2 compositional effects on oil recovery by carbonated water injection. *Ind. Eng. Chem. Res.* **2017**, *56*, 1671–1681. [CrossRef]
19. Hasanvand, M.Z.; Ahmadi, M.A.; Shadizadeh, S.R.; Behbahani, R.; Feyzi, F. Geological storage of carbon dioxide by injection of carbonated water in an Iranian oil reservoir: A case study. *J. Pet. Sci. Eng.* **2013**, *111*, 170–177. [CrossRef]
20. Seyyedattar, M.; Zendehboudi, S.; Butt, S. Molecular dynamics simulations in reservoir analysis of offshore petroleum reserves: A systematic review of theory and applications. *Earth Sci. Rev.* **2019**, *192*, 194–213. [CrossRef]

21. Chen, C.; Wan, J.; Li, W.; Song, Y. Water contact angles on quartz surfaces under supercritical CO_2 sequestration conditions: Experimental and molecular dynamics simulation studies. *Int. J. Greenh. Gas Control* **2015**, *42*, 655–665. [CrossRef]
22. Hu, H.; Li, X.; Fang, Z.; Wei, N.; Li, Q. Small-molecule gas sorption and diffusion in coal: Molecular simulation. *Energy* **2010**, *35*, 2939–2944. [CrossRef]
23. Ma, Z.; Ranjith, P.G. Review of application of molecular dynamics simulations in geological sequestration of carbon dioxide. *Fuel* **2019**, 255. [CrossRef]
24. Zhang, J.; Pan, Z.; Liu, K.; Burke, N. Molecular simulation of CO_2 solubility and its effect on octane swelling. *Energy Fuels* **2013**, *27*, 2741–2747. [CrossRef]
25. Liu, Y.; Lafitte, T.; Panagiotopoulos, A.Z.; Debenedetti, P.G. Simulations of vapor–liquid phase equilibrium and interfacial tension in the CO_2-H_2O-NaCl system. *Aiche J.* **2013**, *59*, 3514–3522. [CrossRef]
26. Makimura, D.; Kunieda, M.; Liang, Y.; Matsuoka, T.; Takahashi, S.; Okabe, H. Application of molecular simulations to CO_2-enhanced oil recovery: Phase equilibria and interfacial phenomena. *SPE J.* **2013**, *18*, 319–330. [CrossRef]
27. Bing, L.; Shi, J.; Wang, M.; Zhang, J.; Sun, B.; Yue, S.; Sun, X. Reduction in interfacial tension of water-oil interface by supercritical CO_2 in enhanced oil recovery processes studied with molecular dynamics simulation. *J. Supercrit. Fluids* **2016**, *111*, 171–178.
28. Plimpton, S. Fast parallel algorithms for short-range molecular dynamics. *J. Comput. Phys.* **1995**, *117*, 1–19. [CrossRef]
29. Berendsen, H.J.C.; Grigera, J.R.; Straatsma, T.P. The missing term in effective pair potentials. *J. Phys. Chem.* **1987**, *91*, 6269–6271. [CrossRef]
30. Harris, J.G.; Yung, K.H. Carbon dioxide's liquid-vapor coexistence curve and critical properties as predicted by a simple molecular model. *J. Phys. Chem.* **1995**, *99*, 12021–12024. [CrossRef]
31. Jorgensen, W.L.; Maxwell, D.S.; TiradoRives, J. Development and testing of the OPLS all-atom force field on conformational energetics and properties of organic liquids. *J. Am. Chem. Soc.* **1996**, *118*, 11225–11236. [CrossRef]
32. Andersen, H.C. Rattle: A "velocity" version of the shake algorithm for molecular-dynamics calculations. *J. Comput. Phys.* **1983**, *52*, 24–34. [CrossRef]
33. Hockney, R.W.; Eastwood, J.W. *Computer Simulation Using Particles*; CRC Press: Boca Raton, FL, USA, 1988.
34. Shinoda, W.; Shiga, M.; Mikami, M. Rapid estimation of elastic constants by molecular dynamics simulation under constant stress. *Phys. Rev. B* **2004**, *69*, 8. [CrossRef]
35. Chattoraj, D.K.; Birdi, K.S. *Adsorption and the Gibbs Surface Excess*; Experimental Methods and Procedures; Springer: New York, NY, USA, 1984.
36. Matsumoto, M.; Kataoka, Y. Study on liquid vapor interface of water. I. Simulational results of thermodynamic properties and orientational structure. *J. Chem. Phys.* **1988**, *88*, 3233–3245. [CrossRef]
37. Rowlinson, J.S.; Widom, B. *Molecular Theory of Capillarity*; Courier Corporation: Honolulu, HI, USA, 1982; 327p.
38. Daniel, R.; Gaddy, V.L. Natural barriers formed in the region of hydrocarbon reservoirs. *Bany. Kohasz Lapok Koolaj Floidgaz* **1972**, *5*, 37–45.
39. Balint, V. Methode de prevision du comportement d'un gisement d'huile balaye par du gaz carbonique. In Proceedings of the Communication 27, Colloque ARTEP, Rueil-Malmaison, France, 7–9 June 1971.
40. Shu, G.; Dong, M.; Hassanzadeh, H.; Chen, S. Effects of operational parameters on diffusion coefficients of CO_2 in a carbonated water-oil system. *Ind. Eng. Chem. Res.* **2017**, *56*, 12799–12810. [CrossRef]
41. Fang, T.; Shi, J.; Sun, X.; Shen, Y.; Yan, Y.; Zhang, J.; Liu, B. Supercritical CO_2 selective extraction inducing wettability alteration of oil reservoir. *J. Supercrit. Fluids* **2016**, *113*, 10–15. [CrossRef]
42. Mohammed, S.; Gadikota, G. The influence of CO_2 on the structure of confined asphaltenes in calcite nanopores. *Fuel* **2019**, *236*, 769–777. [CrossRef]
43. Harris, K.R.; Woolf, L.A. Pressure and temperature dependence of the self diffusion coefficient of water and oxygen-18 water. *J. Chem. Soc. Faraday Trans. 1 Phys. Chem. Condens. Phases* **1980**, *76*, 377–385. [CrossRef]
44. Prielmeier, F.X.; Lang, E.W.; Speedy, R.J.; Lüdemann, H.-D. The pressure dependence of self diffusion in supercooled light and heavy water. *Ber. Bunsenges. Phys. Chem.* **1988**, *92*, 1111–1117. [CrossRef]
45. Bachl, F.; Lüdemann, H.-D. Pressure and temperature dependence of self-diffusion in liquid linear hydrocarbons. *Ztschrift Nat. A* **1986**, *41*, 963–970. [CrossRef]

46. Mohammed, S.; Mansoori, G.A. Molecular insights on the interfacial and transport properties of supercritical CO_2/brine/crude oil ternary system. *J. Mol. Liq.* **2018**, *263*, 268–273. [CrossRef]
47. Wiegand, G.; Franck, E.U. Interfacial tension between water and non-polar fluids up to 473 K and 2800 bar. *Ber. Bunsenges. Phys. Chem.* **1994**, *86*, 809–817. [CrossRef]
48. Georgiadis, A.; Maitland, G.; Trusler, J.P.M.; Bismarck, A. Interfacial tension measurements of the (H_2O + n-Decane + CO_2) ternary system at elevated pressures and temperatures. *J. Chem. Eng. Data* **2011**, *56*, 4900–4908. [CrossRef]
49. Honarvar, B.; Azdarpour, A.; Karimi, M.; Rahimi, A.; Karaei, M.A.; Hamidi, H.; Ing, J.; Mohammadian, E. Experimental investigation of interfacial tension measurement and oil recovery by Carbonated Water Injection: A case study using core samples from an Iranian carbonate oil reservoir. *Energy Fuels* **2017**, *31*, 2740–2748. [CrossRef]
50. Kunieda, M.; Nakaoka, K.; Liang, Y.F.; Miranda, C.R.; Ueda, A.; Takahashi, S.; Okabe, H.; Matsuoka, T. Self-accumulation of aromatics at the oil-water interface through weak hydrogen bonding. *J. Am. Chem. Soc.* **2010**, *132*, 18281–18286. [CrossRef] [PubMed]

Publisher's Note: MDPI stays neutral with regard to jurisdictional claims in published maps and institutional affiliations.

© 2020 by the authors. Licensee MDPI, Basel, Switzerland. This article is an open access article distributed under the terms and conditions of the Creative Commons Attribution (CC BY) license (http://creativecommons.org/licenses/by/4.0/).